

Eric T. da Costa¹
Carlos A. Neves¹
Guilherme M. Hotta¹
Denis T. R. Vidal¹
Marcelo F. Barros¹
Arturo A. Ayon²
Carlos D. Garcia³
Claudimir Lucio do Lago¹

Research Article

Unmanned platform for long-range remote analysis of volatile compounds in air samples

¹Departamento de Química Fundamental–Instituto de Química–Universidade de São Paulo, São Paulo – SP, Brazil

²MEMS Research Laboratory, Department of Physics and Astronomy, The University of Texas at San Antonio, San Antonio, TX, USA

³Department of Chemistry, The University of Texas at San Antonio, San Antonio, TX, USA

Received May 15, 2012

Revised June 11, 2012

Accepted June 11, 2012

This paper describes a long-range remotely controlled CE system built on an all-terrain vehicle. A four-stroke engine and a set of 12-V batteries were used to provide power to a series of subsystems that include drivers, communication, computers, and a capillary electrophoresis module. This dedicated instrument allows air sampling using a polypropylene porous tube, coupled to a flow system that transports the sample to the inlet of a fused-silica capillary. A hybrid approach was used for the construction of the analytical subsystem combining a conventional fused-silica capillary (used for separation) and a laser machined microfluidic block, made of PMMA. A solid-state cooling approach was also integrated in the CE module to enable controlling the temperature and therefore increasing the useful range of the robot. Although ultimately intended for detection of chemical warfare agents, the proposed system was used to analyze a series of volatile organic acids. As such, the system allowed the separation and detection of formic, acetic, and propionic acids with signal-to-noise ratios of 414, 150, and 115, respectively, after sampling by only 30 s and performing an electrokinetic injection during 2.0 s at 1.0 kV.

Keywords:

Capillary electrophoresis-capacitively coupled contactless conductivity detection / Chemical warfare agents / Microchip / Robot / Sampling

DOI 10.1002/elps.201200273

1 Introduction

Because they are independent of the laboratory infrastructure and are able to operate close to the point where the sample is taken, the development of portable instrumentation has gained increasing interest in the recent years [1]. This is particularly important at the industrial and military levels, where not only point-of-care but also real-time analysis is required to assist in the decision-making process. Among others, instruments based on conductimetry [2], potentiometry [3], Raman scattering [4, 5], UV-Vis spectroscopy [6–8], or nuclear magnetic resonance [9] have been recently reported. Although most of these sensors have the potential to detect minute amounts of analytes and have relatively low power requirements, one common shortcoming is their versatility. In this regard, separation-based sensors based on chromatography [10, 11] or CE [12–14] have the capacity to

analyze a larger number of important analytes in the same sample without significant modifications of the hardware. In particular, CE-based sensors offer unparalleled separation efficiency and throughput, require low consumption of power, and can be entirely controlled electronically. In addition, the low volumes involved in typical CE analysis circumvent the necessity to transport large reservoirs of solutions or organic solvents. Such advantages have motivated the development of complete systems, [15–19] integrated procedures, [20] and a series of components for CE, including high-voltage power supplies [21–24] and detectors [25–30].

More recently, the first integrated system capable of performing remote analysis of air samples using microchip-CE was presented [31]. This system (called lab-on-a-robot¹, LOAR¹) was mounted on a battery-operated robotic platform and featured a high-voltage power supply, an electrochemical detector, a wireless modem, a global positioning system, a compass module, and a microactuated pump. Although LOAR¹ was capable of collecting a gas sample, performing the subsequent analysis (injection, separation, and detection), and sending the data to a distant control unit, several electrical connections were exposed, the chip was loosely

Correspondence: Professor Claudimir Lucio do Lago, Instituto de Química–Universidade de São Paulo, Av. Prof. Lineu Prestes 748, CEP 05508-000, São Paulo (SP), Brazil

E-mail: claudemi@iq.usp.br

Fax: +55-11-3091-3781

Abbreviations: CWA, chemical warfare agent; EMPA, ethyl methylphosphonic acid; LOAR, lab-on-a-robot; PMPA, pinacolyl methylphosphonic acid

*Additional corresponding author: Professor Carlos D. Garcia. E-mail: carlos.garcia@utsa.edu

Colour Online: See the article online to view Figs. 1, 3 and 4 in colour.

mounted on top of the platform, the graphical user interface was rather complex, and the autonomy was severely limited by the size of the batteries included. In order to solve these shortcomings, two additional prototypes were designed: LOAR² and LOAR³. This manuscript specifically describes the criteria selected for the fabrication of the components included in LOAR³, the considerations for their integration, and a procedure to analyze an air sample containing a series of organic acids. As such, this paper aims to spark interest in the design of complete hardware platforms to perform unmanned analysis based on microchip-CE.

2 Materials and methods

2.1 Mobile platform and connectivity

In order to provide improved autonomy (with respect to LOAR¹) and generate enough power for all the subsystems, the robot herein described was mounted on an all-terrain vehicle (model ATV-3050C; Coolster, Jinhua, China) equipped with a 110-cm³, four-stroke engine. Although other mobile platforms are currently available in the market (See <http://www.parallax.com/>, <http://www.irobot.com/us/robots/>, and <http://www.qinetiq-na.com/>), the selected vehicle provided a good balance between size, speed, weight, load capacity, and cost. It is also important to note that although only a few modifications were made to the mechanical components, the original electrical system was removed and entirely re-engineered to enable remote control of the vehicle. Additionally, and upon removal of the seat, handlebar, fuel tank, and other parts of the bodywork, a new framework was constructed using aluminum and high-impact polystyrene. The density of these materials considerably reduced the impact of the new structure on the total weight of the vehicle. In fact, the main contribution to the weight was a set of four 12-V, 7-Ah lead batteries (Unipower, São Paulo, Brazil) arranged on each side of the vehicle to maintain the center of gravity. Although these batteries were not essential for the analytical and control systems, they provided a reasonable autonomy and enabled keeping the robot in idle mode, even if the engine is turned off. Figure 1 shows views of the final assembled unit as well as the base station. The dimensions (width × depth × height) of the robot are 72 × 122 × 97 cm (plus 79 cm of the removable antenna).

As they define the data transfer rate, an important aspect to consider is the connectivity between the components of the system. As shown in Fig. 2, a combination of wireless, Ethernet, and USB-enabled connections were selected to define the hardware structure of the robot. For the sake of simplicity, the electric power and mechanical subsystems were not included. Drivability was provided by the driver subsystem, an IP Camera (Wanscam, Shenzhen, China), and a series of sensors that included a global positioning system (GPS) module (LS20031, GPSLOCOSYS Technology, New Taipei, Taiwan), a compass module (HMC6352, Parallax, Rocklin, CA, USA), two gyroscope

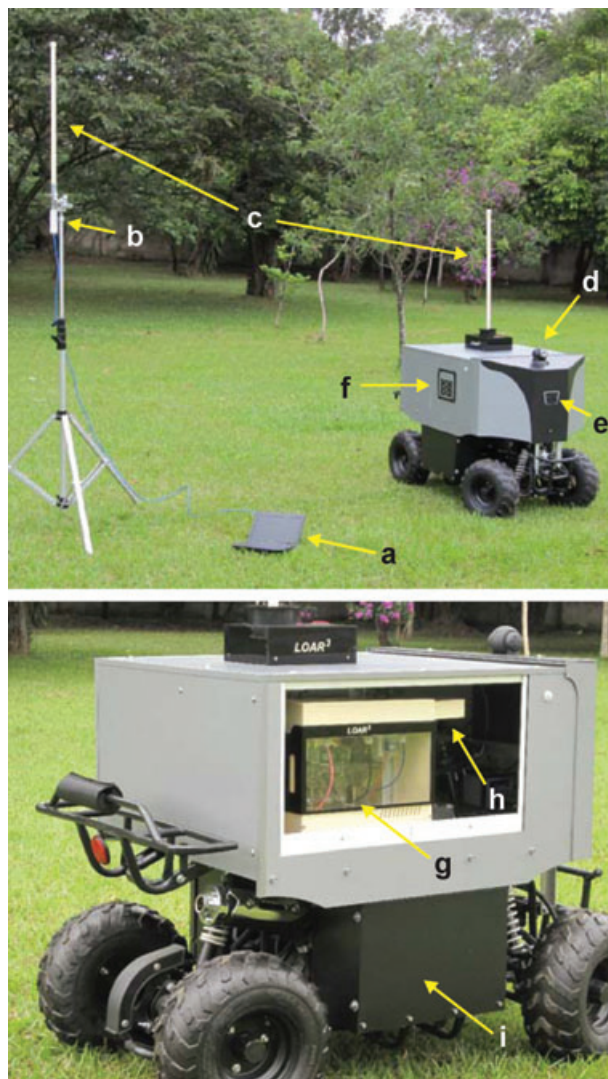


Figure 1. Top image: Picture of the remotely controlled vehicle and base station including a notebook (a), the high-power wireless access point (b), a high-gain Wi-Fi antenna (c), the wired network IP camera (d), the IR distance sensor (e), and the window for air sampling (f). Bottom image: close view of the electrophoresis system inside the vehicle (g), location of the air intake for the electrophoresis system (h), and one of the battery packs (i). All other sensors were installed inside the case to protect them from the environment.

modules (IXZ-650 and IDG-650; InvenSense, Sunnyvale, CA, USA), infrared (IR) distance sensor (GP2Y0A02YK0F, Sharp, Camas, WA, USA), and a 3-axis orientation sensor (MMA7660FC, Freescale Semiconductor, Austin, TX, USA).

The remote station was built on an Intel Atom-based motherboard (D945GCLF2D, Intel, Santa Clara, CA, USA) running Ubuntu Linux as its operating system. This platform was selected because of its low power requirements, lightweight, small form factor, and low dissipated heat. The subsystem's head and driver, the electrophoresis module, and the detection system (vide infra) were controlled by

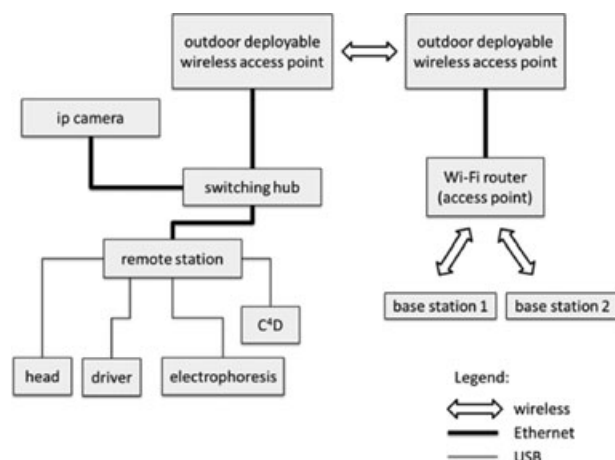


Figure 2. System hardware and connectivity diagram. The Wi-Fi router provides connection of the base station devices to the high-power bridge. Although two base stations are shown in the diagram, only one computer was required for remote control and data acquisition. The selected architecture enables the integration of other clients such as smartphones or other devices compatible with IEEE802.11b, g, or n protocols.

USB-based Teensy 2.0 modules (PJRC, Sherwood, OR, USA), which is based on the ATMEGA32U4 microcontroller (Atmel, San Jose, CA, USA). The vehicle-embedded computer and IP camera were connected to the base station through a high-power (800 mW) wireless access point (Bullet 2HP, Ubiquiti Networks, San Jose, CA, USA) and a high-gain omnidirectional antenna (Hypersat Omni 12 dBi, Sat5, Pará de Minas, Brazil). A similar access point and antenna configuration were used in the base station, providing a maximum link distance between the robot and the base station of 5 miles (outdoors).

Communication between the internal subsystems and the vehicle-embedded computer (remote station) was implemented as an ASCII string-based protocol, encoded in TCP/IP datagrams to enhance the compatibility with current network protocols. With the exception of the aforementioned subsystems, all other hardware and communication protocols were assembled using conventional parts for wired and wireless Ethernet.

2.2 Analytical subsystem

As schematically shown in Fig. 3, the analytical subsystem comprised three compartments: sampler, electrophoresis, and terminator. The dimensions of this subsystem were $31 \times 29 \times 25$ cm in width, depth, and height, respectively. The first compartment (sampler) included a 7.5-mL glass reservoir containing the background electrolyte (BGE), an air pump (model KPM12C, Xiamen Koge Micro Tech, Xiamen, China), a 12-cm segment of polypropylene Oxyphan PP50/200 tube (200 μm id, 300 μm od, and wall porosity 200 nm; Membrana, Wuppertal, Germany), and a waste reservoir. When the air pump was turned on, pressure built in the reservoir

containing the BGE, displacing the solution inside the porous tube at an approximate flow rate of 0.9 mL/min. An ad hoc interface between the Oxyphan tube and a fused-silica capillary (Polymicro, Phoenix, AZ, USA) allowed the injection of discrete sample volumes on the capillary inlet. The remaining solution was then pumped through a series of chambers before reaching the chamber containing a stainless steel electrode. This electrode was connected to the ground pole of an adjustable 30-kV high-voltage power supply (model 30A12-P4-STD, Ultravolt, Long Island, NY, USA). After passing through a servo-controlled valve, the solution was discarded into the waste reservoir. When closed, the servo valve allowed the injection of sample or the BGE into the capillary. This procedure was selected because it allowed the hydrodynamic injection of the sample as well as BGE, used to implement a rinsing step after each analysis.

The second compartment of the analytical subsystem (CE) contained a fused-silica capillary and a grounded 6-mm thick aluminum block, thermostated using a 60-W, 15-V Peltier element (Danvic, São Paulo, Brazil). In order to allow proper heat dissipation, the capillary was pressed against the flat surface of the aluminum block. A previously described capacitively-coupled contactless conductivity detector (C^4D) [32, 33] was positioned close to the end of the capillary in an ad hoc slot made in the aluminum block. Besides the advantages traditionally offered by C^4D [32, 34], this detection system was selected because it enabled the detection of multiple analytes and its integration with the system with relatively few modifications in the hardware. The output signal of the detector was sequentially filtered by a 3-point windowed median filter [35] and a three-point windowed moving average filter. It is also worth noting that although the design of the terminator block was simpler than the sampler (containing the porous tube and the servo valve), this block required better electrical insulation. The main reason for this difference is that the terminator block was used to apply the high voltage to the fused-silica capillary. Both the sampler and terminator blocks were laser machined (cut or engraved) and thermally bonded according to the procedure described in Section 2.3.

In order to capture air samples, a brushless 12-V fan was incorporated in the sampler block. This fan was used to direct a stream of air from the robot's surroundings to the Oxyphan tube in the sampler. This fan as well as the pumps, the servo valve, and the high-voltage power supply were sequentially operated by the microcontroller, which also allowed the implementation of different procedures for sampling, analysis, and rinsing.

2.3 Cutting and sealing of PMMA fluidic parts

A Gravograph LS-100 laser cutter and engraver (La Chapelle-St Luc, France) was used to produce channels, chambers, and holes in PMMA as well as to cut plastic hardware pieces. The ablation depth and width was controlled by the laser power, the scanning velocity of the cutting head, and the focal plane of the beam. For example, when the CO_2 laser beam (3 W)

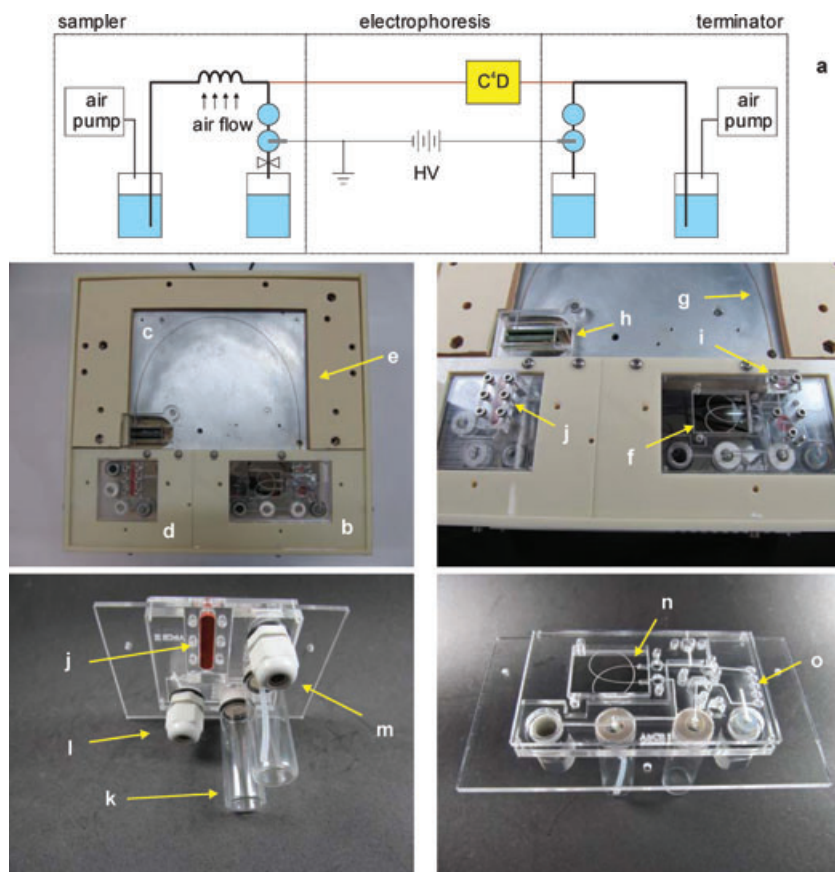


Figure 3. Schematic diagram of the analytical subsystem. The main regions shown in the block diagram (a) are the sampler (b), electrophoresis (c), and terminator (d). A thermal insulator (e) was used to fill the region around the aluminum block. The thermoelectric cooling system was positioned on the bottom face of the block (thermal-insulated cover not shown). The sampler contained a window (f) through which the air flowed. The fused-silica capillary (g) was positioned on the aluminum block. The C⁴D (h) was positioned at the end of the capillary, which was connected to the sampler and terminator through silicone septa (i, j). The solutions were kept in glass reservoirs (k). A gland connector (l) was used to seal the contact to the high-voltage electrode. Another gland connector (m) was used for coupling of the tube from the air pump. The Oxyphan tube (n) was positioned in the sampler window. Pockets (o) were used to implement the separated electrolysis approach (see Section 3.2).

was focused on the surface of the substrate, and the scan rate was set to 20 mm/s, channels widths of 150 μm were produced. Channels with different aspect ratios were produced by a combination of increased power (up to 30 W) and the adjustment of the focal plane of the laser beam. For instance, a 15 W laser beam tracking at 40 mm/s, focused 5 mm above the surface yielded 550 μm wide channels. As a representative example, Fig. 4 shows the images used to cut and engrave the sampler and terminator compartments. The laser conditions defined for *seq6* and *seq7* were defined to cut through the 3 mm PMMA plate. Thus, *seq6* defines holes in the pieces, which are used to access the fluidic channels and fixation. The channels in the terminator compartment, defined by *seq2*, were used to provide openings for the reservoirs connected to the high-voltage power supply. In order to minimize the probability of arcing (due to the application of the high voltage during the electrophoresis step), these reservoirs were defined to be as large as possible. The regions made with *seq1* and *seq5* formed reservoirs for separated electrolysis [36].

Also as a representative example, Fig. 5 shows a close view of a typical profile for a channel obtained when the laser beam was focused at 5 mm above the surface (*seq3* in Fig. 4). At the edge of the PMMA block, the fused-silica capillary was introduced in this triangular channel (f, in Fig. 4) and sealed with the aid of a silicone septum. The two parts of the

septum were pressed against each other by two PMMA pieces and secured using screws. The location for the openings for the septa in the sampler compartment and in the terminator is shown in Figs. 3 and 4.

Although most fluidic circuits do not demand minimum dead volumes (that can be achieved by using narrow, shallow channels), such devices must be properly sealed to avoid leakages. Therefore, PMMA layers were sealed using a combination of pressure (590 kPa), temperature (110°C), and time (40 min). This temperature was selected because it is close to the glass transition temperature of PMMA. After 40 min, the resulting pieces were removed from the oven and allowed to cool-down to room temperature while keeping the pressure to prevent the deformation of the block. Although the channels were formed between only two pieces of PMMA, other layers were added to provide structural support, connections, and reservoirs (see Fig. 3). Epoxy glue (Araldit, Brascola, São Bernardo do Campo, Brazil) was used to fix other parts to the PMMA blocks.

Two 15 mm long, 0.3 mm od stainless steel tubes were used to couple the Oxyphan tube to the microfluidic channels of the sampler. These tubes were obtained by removing the epoxy glue and the luer lock connector from standard insulin needles. As previously described by Coelho and Gutz [37], a Tygon sleeve was used to join the Oxyphan and stainless steel tubes.

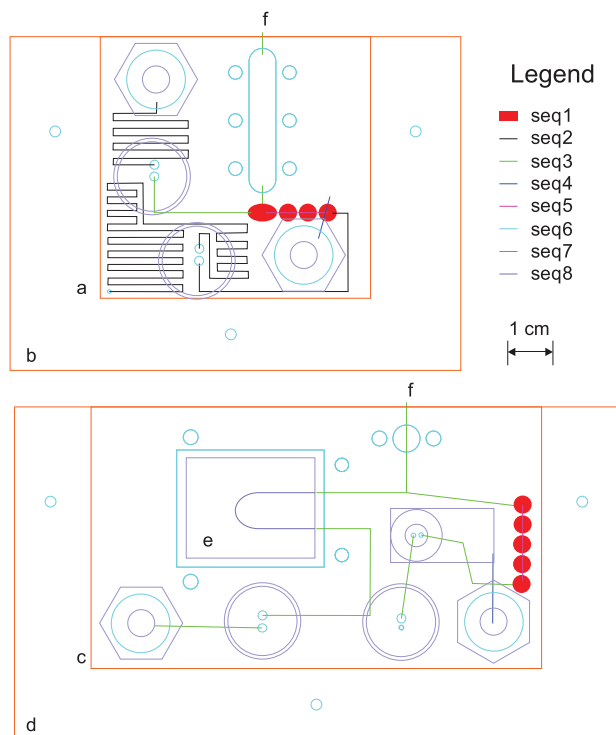


Figure 4. Drawings for laser cutting and engraving of the sampler and terminator. Each block was composed of two pieces of PMMA, sealed to form the channels. In this figure, these pieces were overlaid to facilitate the visualization of the fluidic circuit. The terminator was composed by the pieces (a) and (b), while the sampler was composed by (c) and (d). Both pieces of the sampler contained a window *e*, where the Oxyphan tube was placed. The fused-silica capillary was coupled through channels (f). The laser machine executed tasks (schematically shown as different colors) according to the sequences from *seq1* to *seq7*. The drawings in color defined by *seq8* were only used for visual alignment of the pieces and were ignored by the laser machine. Each color shown in the legend corresponds to a unique set of four parameters: laser power (W), velocity (mm/s), distance between the surface and the focal point (mm), and mode. The parameters for *seq1* to *seq7* were (12, 225, -7, raster), (3, 10, 0, vectorial), (30, 14, -5, vectorial), (16, 10, -8, vectorial), (3, 20, 0, vectorial), (30, 12, 0, vectorial), and (30, 12, 0, vectorial), respectively. For the sake of visualization, other details related to the fixation, were not included in the figure.

2.4 Reagents and solutions

Acetic and nitric acids were obtained from Synth (Diadema, Brazil). Sodium bicarbonate, sodium carbonate as well as formic, propionic, hydrochloric, and sulfuric acids were obtained from Merck (Darmstadt, Germany). MES, L-histidine (His), CTAB, ethyl methylphosphonic acid (EMPA), and pinacolyl methylphosphonic acid (PMPA) were purchased from Sigma (St. Louis, MO, USA). All aqueous solutions were prepared using 18 M Ω -cm deionized water (Barnstead/Thermolyne, Dubuque, IA, USA). The MES/His BGEs were prepared with equimolar amounts of the free acid and the free base. The bicarbonate BGE was 20 mmol/L in

each Na₂CO₃ and NaHCO₃. In all cases, 0.2 mmol/L of CTAB was added to revert the EOF.

3 Results and discussion

The electrophoresis system here introduced can be classified as a hybrid instrument, because the sampler and the terminator sectors are microfabricated in PMMA while a fused-silica capillary was used for the electrophoretic separation. The hypothesis was that such hybrid approach would enable coupling some of the advantages of simple microfabrication techniques and the high separation efficiency obtained in fused-silica capillaries.

3.1 Considerations related to the fused-silica capillary

One important aspect to rationally improve the performance of the proposed instrument is the evaluation of the effect that relevant variables have on the number of theoretical plates (*N*). In our case, this analysis was performed according to Eq. (1),

$$N = \frac{L_D^2}{\frac{2k_B T L_D L_T}{z e V} + \frac{(\Delta x_i)^2}{12} + \frac{(\Delta x_d)^2}{12}} \quad (1)$$

where L_T is the total length of the capillary, L_D is the effective length of the capillary, k_B is the Boltzmann constant, T is temperature, z is the charge of the ion, e is the elemental charge, V is the applied voltage, Δx_i is the extension of the capillary occupied by the sample, and Δx_d is the extension of the capillary covered by the detector. This equation shows that when L_D is shorter than L_T and when Δx_i and Δx_d are finite, the length of the capillary becomes critical to increase the number of theoretical plates. It is also well known that, in order to prevent electrically shunting the signal to the ground [32, 38], the C⁴D should be as far as possible from the outlet of the capillary, limiting L_D and therefore implying that L_D would always be shorter than L_T . This BGE-filled segment of the fused-silica capillary between the outlet reservoir and the detector allows the development of an impedance value that is significantly larger than the impedance of the conductivity cell. Consequently, the optimum position for the detector (distance from the end of the capillary, $L_T - L_D$) depends on several factors such as the inner and the outer diameters of the capillary, the operating frequency, and the conductivity of the BGE [38] and should be defined considering a balance between the separation efficiency and the performance of the C⁴D. Therefore, and although this balance can be reached with a few centimeters (under typical experimental conditions), a distance of 6.4 cm ($L_T - L_D$) was selected as optimum for this instrument.

Two additional parameters were also considered in the design of the analytical subsystem: Δx_i and Δx_d (defining the distance between the electrodes of the C⁴D). In

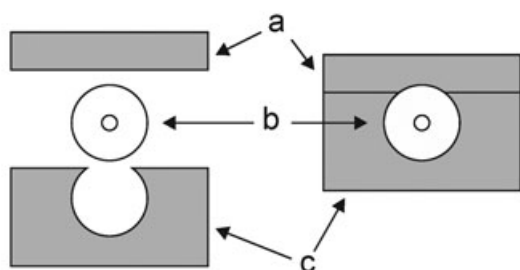
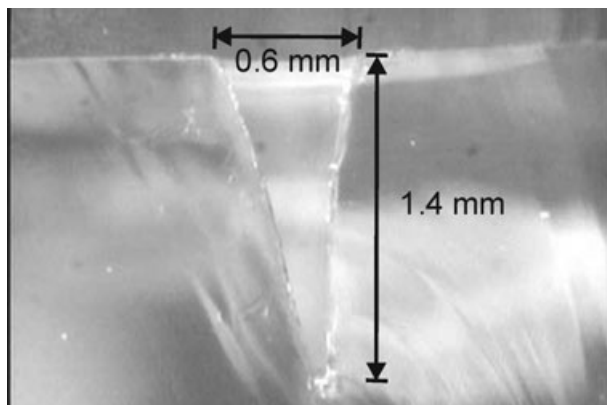


Figure 5. Channel profile obtained by laser machining (30 W and 14 mm/s, focused 5 mm above the PMMA surface). A 360- μm od fused-silica capillary can be easily wedged inside the channel for coupling it to the PMMA microfluidic modules. Although the cylindrical profile of the capillary did not match the triangular profile of the channel, a septum composed of two layers of silicone (a and c in the diagram) allowed the correct sealing of the fluidic parts and the fused-silica capillary (b).

agreement with a previous report [33], that distance was selected to be 0.5 mm. Thus, taking into account the migration of a monocharged analyte when 10 kV is applied, Equation 1 suggests that a 58-cm long capillary will have 90% of the maximum possible efficiency (estimated for an infinitely long capillary). Developing microfabricated structures with such lengths undoubtedly possesses a series of technical challenges. Therefore, and in order to couple the advantages of microfluidic devices with those obtained with conventional fused-silica capillaries and C^4D [34], a series of PMMA components were designed and integrated in LOAR³.

3.2 Considerations related to the PMMA components

As previously stated, PMMA components were implemented to perform sample handling operations. In order to enable the partition of the components from air into the BGE, an Oxyphan tube was integrated in the PMMA sampler module. This material was selected because this hydrophobic polymer contains pores (of about 200 nm) that allow an effi-

cient exchange of gases without leakage of aqueous solutions [37, 39, 40]. It was observed, however, that the addition of surfactants to the BGE (such as CTAB 0.2 mmol/L) produced significant decreases in surface tension, yielding to the formation of solid deposits on the outer surface of the tube. Although the formation of crystals was only evident after 24 h of operation, which largely exceeded the normal operational time of the robot, the tube was periodically replaced to minimize any potential effect on the performance of the sampler.

Besides the afore-mentioned advantages in throughput and cost, the combination of laser machining and PMMA enabled the integration of a series of pockets (see regions defined by *seq1* in Fig. 4), which were filled with BGE and allowed the implementation of the separated electrolysis [36]. To the best of our knowledge, this is the first time that such an approach is implemented at the microchip scale. The basic idea is to separate the region around the electrode and the end of the capillary by at least a couple of wide-bore and narrow-bore fluidic segments. Although the narrow-bore segments (defining the connections between the pockets depicted by *seq5* in Fig. 4) are efficient barriers to the diffusion of species electrochemically transformed on the surface of the electrode, they are not effective to prevent contamination by migration. This is because of the presence of the high-electric field inside the narrow bore. The wide-bore regions, on the other hand, are very effective to prevent the transport by migration, although they are less effective against transport by diffusion. Thus, and as it was previously demonstrated [36], a combination of wide- and narrow-bore regions was considered appropriate and included in the design of the system. Although the implementation of this approach requires additional parts, and could in some cases become cumbersome [41], the present fabrication strategy demonstrates that separated electrolysis can be implemented at the microchip scale and provide significant improvements in stability.

3.3 Considerations related to the solid-state heat dissipation

One of the advantages of using fused-silica capillary instead of channels made polymeric materials is the superior thermal conductivity of silica ($1.4 \text{ W m}^{-1} \text{ K}^{-1}$). Although these capillaries are coated with an external layer of polyimide, which has a smaller thermal conductivity ($0.5 \text{ W m}^{-1} \text{ K}^{-1}$) than silica, the limited thickness of this layer does not significantly affect the heat exchange with the environment. In general, the heat from the external surface of the capillary can be dissipated in different ways. Although the most common approach is the use of a circulating fluid (air or a special liquid), a solid-state approach based on an aluminum block and a 60-W, 15-V Peltier element was implemented in LOAR³. Besides being coupled to the Peltier element, Al is high-thermal conductivity material ($237 \text{ W m}^{-1} \text{ K}^{-1}$) and facilitated the dissipation of heat produced in the capillary. In order to maximize the heat transfer from the capillary to the aluminum block, the

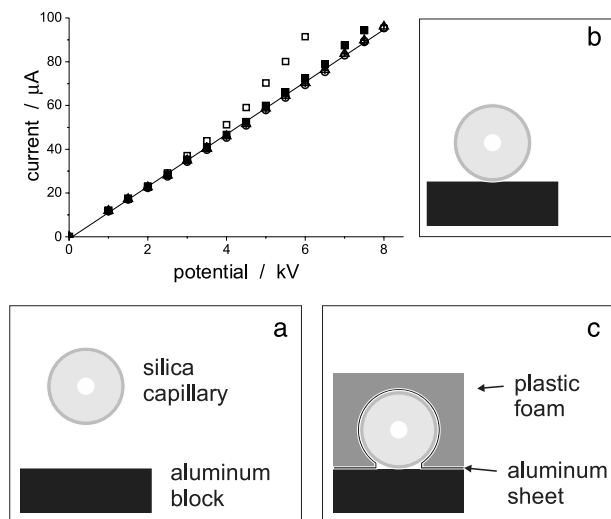


Figure 6. Current voltage curves for the heat dissipation approaches are described in the manuscript. When the capillary was suspended in air as shown in a, a clear non-Ohmic behavior was observed (open square). The simple contact with the aluminum surface (b) significantly improved the heat transfer (solid square). However, better results were obtained when aluminum foil was pressed against the capillary as shown in c (triangle). The linear fit for the crosses is shown.

performance of three strategies was evaluated by performing current-voltage curves using a 75 μm id capillary filled with KCl 100 mmol/L. Although this solution had a conductivity that was considerably higher than those ones used with C^4D , it represented a limiting case that would validate the results obtained under routine conditions. The results are summarized in Fig. 6. For comparison purposes, the results obtained for the case where the capillary was suspended in the air were also included in the figure.

As it can be observed, clear deviations of the Ohmic behavior were obtained when the capillary was suspended in air. Although the heat transfer was significantly improved by the simple contact between the fused-silica capillary and the surface of the aluminum block, much improved results were obtained when the capillary was covered with a sheet of aluminum foil (10 μm thick) and pressed against the block by a piece of polystyrene foam. Although the polystyrene foam has low thermal conductivity (0.033 $\text{W m}^{-1} \text{K}^{-1}$), it improved the contact between the capillary and the aluminum pieces, therefore facilitating the heat transfer. Other materials such as zinc-based thermal grease IPT (0.4 $\text{W m}^{-1} \text{K}^{-1}$, Implastec, Votorantim, Brazil) and silver-based thermal grease TG-2 (1.5 $\text{W m}^{-1} \text{K}^{-1}$, Thermaltake, Beijing, China) were also investigated, but no further improvements in the performance were observed. In addition, when Joule heating curves were obtained in a regular instrument with air cooling system and using the same capillary and BGE, similar results were obtained (data not shown). In this case, the voltage and current were limited by either the capacity of the high-voltage power supply or the formation of bubbles inside the capillary, which

are most likely to occur in low-thermal conductivity regions (connections or inside the PMMA blocks).

Besides requiring little additional space, the solid heat sink has the potential to provide excellent thermal stability to the system with no moving parts and a solid support to immobilize the capillary, therefore improving the mechanical strength of the setup. As the aluminum block can be electrically grounded, it can also improve the reproducibility of the EOF [42, 43]. Such advantages are not only important to field instruments, but also to benchtop instruments.

3.4 Considerations related to the detection of chemical warfare agents (CWAs)

It is well known that CWAs based on organic phosphonates undergo hydrolysis [44], releasing a variety of organic acids. In particular, alkyl alkylphosphonic acids resulting from the first hydrolysis of G- and V-type nerve agents quickly can be used to trace the release of CWA by a variety of methods, including CE- C^4D [45–47]. Therefore, and because real CWAs were not considered appropriate for this exercise, the analysis of the degradation products of CWAs was modeled through a sequence that includes a preconcentration step (at the Oxyphan membrane filled with an alkaline BGE), a hydrodynamic injection, separation by capillary electrophoresis and detection by C^4D . The paper by Ding et al. [48] was used as the starting point for the development of the analytical method. Although, the authors demonstrated that it was possible to separate isopropyl methylphosphonic acid, PMPA, EMPA, and methylphosphonic acid along a 6.5 cm long channel and to detect them using a C^4D detector, using 5 mmol/L MES/His as the BGE, other ionic species (such as chloride, sulfate, and nitrate) should be also considered when air is sampled. Additionally, formate and acetate may be released by partial oxidation of fuels [49]. More importantly, the most abundant anionic species in the sampled mixture should be bicarbonate, which is formed by hydration and ionization of atmospheric CO_2 at the alkaline BGE in the sampler.

Consequently, the separation conditions were optimized using standard solutions of the corresponding salts or acids. These experiments were carried out in a CE- C^4D instrument described elsewhere [42], which was equipped with two conductivity detectors [33]. Figure 7 shows the electropherograms at the first and second detectors when the BGE is MES/His (pH 6.1). As it can be observed, the efficiency was better than that one obtained by Ding et al. [48], because of the size of the capillary. It is worth noting that, although only two phosphonates (PMPA and EMPA) were available, these two species are the fastest and slowest species in this family, therefore enabling the comparison with other anionic species. The electropherogram at the first detector shows that baseline resolution is obtained for the separation of PMPA and EMPA in less than 1 min. Although this was considered acceptable for a generic identification of CWAs, the 5-min run (obtained with the second detector) allowed the identification of different CWAs with mobilities between those ones

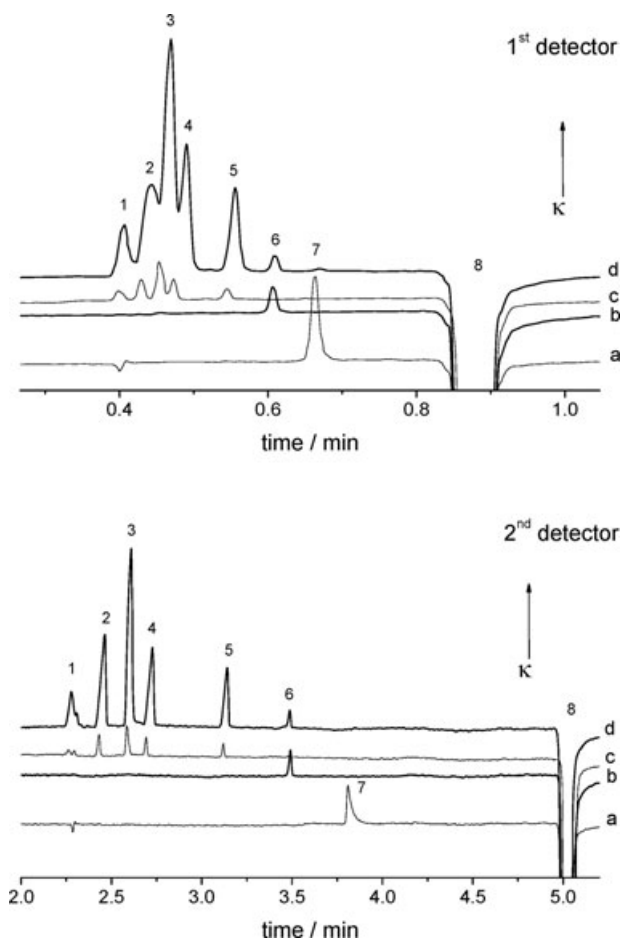


Figure 7. Electropherograms obtained at the first and second detectors for synthetic mixtures containing: chloride (1), nitrate (2), sulfate (3), formate (4), acetate (5), EMPA (6), and PMPA (7). Peak 8 is the so-called EOF peak or water peak. The samples were: a–PMPA 2 mmol/L; b–EMPA 300 $\mu\text{mol/L}$; c–all species but EMPA and PMPA at 100 $\mu\text{mol/L}$; d–EMPA 200 $\mu\text{mol/L}$, PMPA 100 $\mu\text{mol/L}$, and 1 mmol/L for the other species. A 50- μm id and 77-cm long fused-silica capillary was used. The detection points were 11 cm (first detector) and 66 cm (second detector). The BGE was MES/His 30 mM (pH 6.1) with 0.2 mM CTAB at 25°C. The sample was hydrodynamically injected by 3 s at 3.5 psi and high voltage was 25 kV.

for PMPA and EMPA. Despite the good separation, there are three important points to be considered:

- (i) The pH of the running electrolyte is not ideal for the capture and hydrolysis of the CWAs. In this case, two fluidic paths should be incorporated in the manifold: one for sampling (at high pH) and other for running (MES/His pH 6.1).
- (ii) Although a peak for bicarbonate is not observable, its mobility at pH 6.1 leads to a “system peak” close to the peak corresponding to PMPA. This system peak can be observed when the running electrolyte is exposed to the air for several minutes.

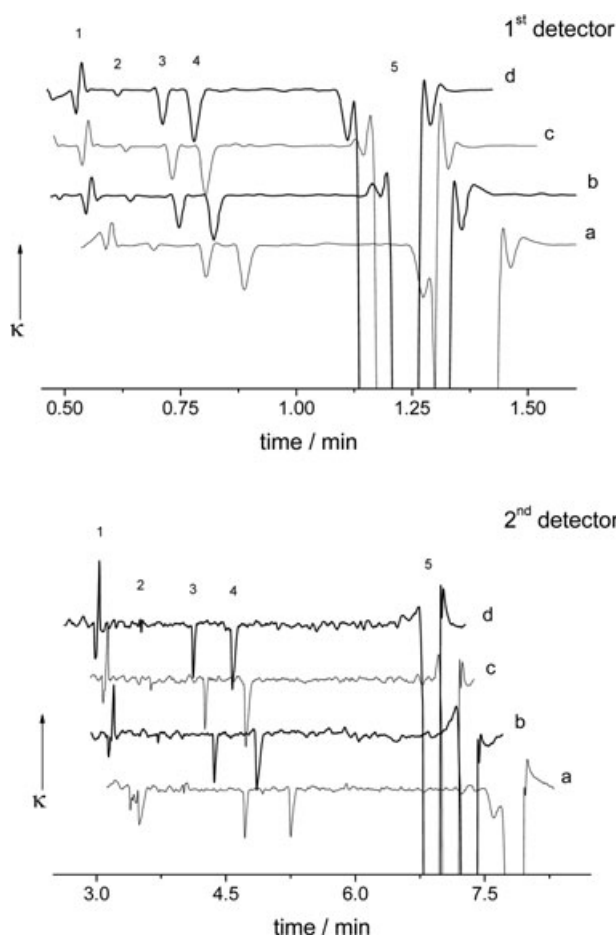


Figure 8. Electropherograms obtained at the first and second detectors for synthetic mixtures containing: chloride, nitrate, sulfate, formate, bicarbonate, acetate (2), EMPA (3), and PMPA (4). Peak 1 is a system peak due to the presence of bromide in the BGE, and peak 5 is the EOF peak. The samples were composed of 200 μM in PMPA and EMPA and 100 μM for the other anions. A 50 μm id and 77-cm long fused-silica capillary was used. The detection points were 11 cm (first detector) and 66 cm (second detector). The running buffer was $\text{Na}_2\text{CO}_3/\text{NaHCO}_3$ (pH 10.2) with 0.2 mM CTAB. The sample was hydrodynamically injected by 3 s at 3.5 psi and high voltage was 25 kV. The temperatures were 20°C, 25°C, 30°C, and 35°C from electropherograms from A to D, respectively.

- (iii) Although MES has lower mobility than the phosphonates yielding to positive peaks for the phosphonates, the sensitivity was low. This sensitivity could be improved by selecting a buffer with a mobility either lower or higher than MES. The latter would result in negative peaks [38].

Consequently, a BGE composed of $\text{Na}_2\text{CO}_3/\text{NaHCO}_3$ (pH 10.2) was considered more appropriate. As this solution contains bicarbonate (a high mobility anion), it not only rendered negative peaks for all the analytes, but also addressed the previously described problems associated with MES/His buffers.

Figure 8 shows the electropherograms obtained with a synthetic mixture of the selected organic acids plus other

anions of interest. Chloride, nitrate, sulfate, formate, and bicarbonate were not detected because bicarbonate is the co-ion in BGE, which reduces the sensitivity for these high-mobility species. A small peak for acetate was still observed. The low sensitivity for the high mobility species was not considered a problem, as they are not related to the analytes of interest. Although not obtained from the direct degradation of CWAs and can only be considered as a general reference, the LODs ($S/N = 3$) for EMPA and PMPA were ca. 10^{-5} mol/L, which is in good agreement with other reports [34]. As shown in Section 3.5, if required, the sampling can be dynamically handled in order to improve the sensitivity.

Figure 8 also shows the effect of temperature on the separation of the selected organic acids. Due to the increase in mobility and decrease in viscosity, a slight reduction in the migration time of all peaks was observed. Since neither the signal-to-noise ratio nor the efficiency was affected, it was concluded that the analysis can be seamlessly performed at any operational temperature within the investigated range. This feature is also important to determine the configuration of the thermal control of the instrument as maintaining a narrow temperature range (especially at higher exterior temperatures) would require more power. Consequently, unless extreme conditions are present, the power-saving setting (operation at room temperature) can be utilized.

3.5 Detection of volatile carboxylic acids

In agreement with previous literature reports specifically targeting the analysis of degradation products of CWAs [45–47], the results described in the previous section demonstrated that the hydrolysis products of CWAs could be electrophoretically separated from other common species present in air in a single-line manifold, as shown on Fig. 4. Therefore, and in order to demonstrate the functionality of the porous membrane, the sampling of formic, acetic, and, propionic acids was investigated. Although these compounds are not related to the degradation products of CWAs, they were selected because they represent an appropriate model to probe the performance of LOAR³. For these experiments, a beaker (1.5 cm diameter) containing 25% v/v solutions of either (i) DI water, (ii) acetic acid, (iii) acetic and formic acids, or (iv) acetic, formic, and propionic acids was positioned at 1 cm from the sampler fan. For each sampling step, the fan was turned on for 30 s. Then, a plug of solution was pumped from the sampler compartment to the inlet of the capillary, and electrokinetically injected (2.0 s at 1 kV). After the sample was pumped out (to the waste reservoir) and a fresh portion of BGE was positioned in front of the capillary end, the electrophoretic run was carried out at 10 kV. Based on the experiments described in 3.4 and the composition of the sample, MES/His 20 mmol/L (pH 6.1) plus CTAB 0.2 mmol/L was selected as the background electrolyte. The resulting electropherograms (collected using the remote station) are shown in Fig. 9.

For the sampling conditions used in the present experiment, the signal-to-noise ratios for formate, acetate, and propionate were 414, 150, and 115, respectively. It is worth noting that if higher sensitivity is required, the sampling time (> 30 s) and the injection parameters (time and potential) can be further optimized.

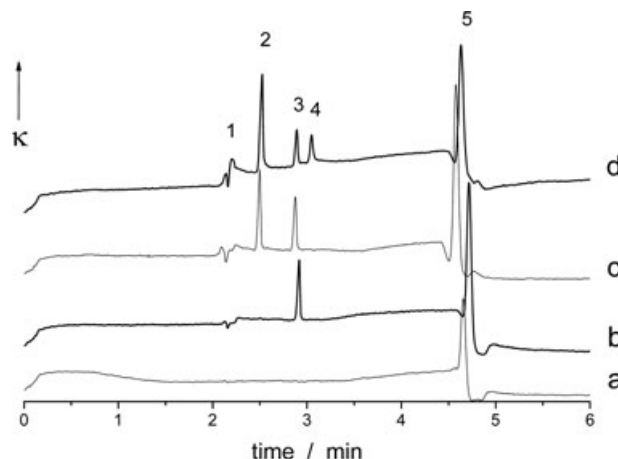


Figure 9. Electropherograms obtained upon the injection of air samples collected through Oxyphan tube: (a) pure water and aqueous solutions of (b) acetic acid, (c) acetic and formic acids, and (d) acetic, formic, and propionic acids at 25% (v/v). The vapor phase was vented over the Oxyphan tube by 30 s, and then electrokinetically injected by 2.0 s at 1.0 kV. The electropherograms were obtained at 10 kV. The peaks were attributed to bromide (1) (system peak resulting from the use of CTAB in the BGE), formate (2), acetate (3), propionate (4), and EOF (5).

It is worth noting that if higher sensitivity is required, the sampling time (> 30 s) and the injection parameters (time and potential) can be further optimized.

4 Concluding remarks

Although testing degradation products of real CWAs is clearly beyond our capacity, the results described in the preceding sections provide strong evidence supporting the capabilities of the developed instrument to detect organic acids in air samples. To develop this instrument, a modular approach was adopted, where the functionality of the different parts was first demonstrated individually and then collectively assessed. Besides demonstrating the capacity of the system to perform the first remotely controlled analysis of organic acids using CE-C⁴D, this paper (i) described the advances in the development of a solid-state heat dissipation strategy, which can be applied to any other capillary electrophoresis system, (ii) demonstrated that separated electrolysis can be implemented at the microchip scale, and (iii) presented a combination of fused-silica capillary and PMMA-based microfabrication. The latter is an interesting approach that combines the high efficiency of a conventional fused-silica capillary with the flexibility, simplicity, and throughput of laser micromachining.

Authors thank Office of Naval Research Global (Grant Number N62909-10-1-7043), Professor Dr. Lucio Angnes for the CO₂ laser facility, and Professor Dr. Ivano G. R. Gutz for the samples of Oxyphan tube. CLL and GMH thank CNPq for the fellowship.

ETC thanks CAPES for the fellowship. DTRV thanks FAPESP for the fellowship.

The authors have declared no conflict of interest.

5 References

- [1] Lee, M., Cho, K., Yoon, D., Yoo, D. J., Kang, S. H., *Electrophoresis* 2010, **31**, 2787–2795.
- [2] Chai, C., Liu, G., Li, F., Liu, X., Yao, B., Wang, L., *Anal. Chim. Acta.* 2010, **675**, 185–190
- [3] Yunus, S., Attout, A., Vanlancker, G., Bertrand, P., Ruth, N., Galleni, M., *Sens. Actuators B* 2011, **156**, 35–42.
- [4] Quang, L. X., Lim, C., Seong, G. H., Choo, J., Do, K. J., Yoo, S.-K., *Lab. Chip* 2008, **8**, 2214–2219.
- [5] Guzmán, E., Baeten, V., Pierna, J. A. F., García-Mesa, J. A., *Talanta* 2012, **93**, 94–98.
- [6] Camou, S., Shimizu, A., Horiuchi, T., Haga, T., *Procedia Chem.* 2009, **1**, 1495–1498.
- [7] de Vargas-Sansalvador, I. M. P., Fay, C., Phelan, T., Fernández-Ramos, M. D., Capitán-Vallvey, L. F., Diamond, D., Benito-Lopez, F., *Anal. Chim. Acta.* 2011, **699**, 216–222.
- [8] Salmerón, J. F., Gómez-Robledo, L., Carvajal, M. Á., Huer-tas, R., Moyano, M. J., Gordillo, B., Palma, A. J., Heredia, F. J., Melgosa, M., *J. Food Eng.* 2012, **111**, 247–254.
- [9] Perlo, J., Demas, V., Casanova, F., Meriles, C. A., Reimer, J., Pines, A., Blümich, B., *Science* 2005, **308**, 1279.
- [10] Kiplagat, I. K., Kubáň, P., Pelcová, P., Kubáň, V., *J. Chromatogr. A* 2010, **1217**, 5116–5123.
- [11] Kutter, J. P., *J. Chromatogr. A* 2012, **1221**, 72–82.
- [12] Kaigala, G. V., Hoang, V. N., Stickel, A., Lauzon, J., Manage, D., Pilarski, L. M., Backhouse, C. J., *Analyst* 2008, **133**, 331–338.
- [13] Ryvolová, M., Macka, M., Preisler, J., *TrAC Trends Anal. Chem.* 2010, **29**, 339–353.
- [14] Yuan, L., Wei, H., Feng, H., Li, S., *Anal. Bioanal. Chem.* 2006, **385**, 1575–1579.
- [15] Herr, A. E., Molho, J. I., Santiago, J. G., Kenny, T. W., Borkholder, D. A., Kintz, G. J., Belgrader, P., Northrup, M. A., *Micro Total Analysis Systems 2000, Proceedings of the mTAS Symposium, 4th, Enschede, Netherlands, May 14–18, 2000*, 367–370.
- [16] Kappes, T., Galliker, B., Schwarz, M. A., Hauser, P. C., *TrAC Trends Anal. Chem.* 2001, **20**, 133–139.
- [17] Kappes, T., Hauser, P. C., *Anal. Com.* 1998, **35**, 325–329.
- [18] Shrinivasan, S., Norris, P. M., Landers, J. P., Ferrance, J. P., *J. Assoc. Lab. Autom.* 2006, **11**, 254–259.
- [19] Chiesl, T. N., Chu, W. K., Stockton, A. M., Amashukeli, X., Grunthaner, F., Mathies, R. A., *Anal. Chem.* 2009, **81**, 2537–2544.
- [20] Mora, M. F., Greer, F., Stockton, A. M., Bryant, S., Willis, P. A., *Anal. Chem.* 2011, **83**, 8636–8641.
- [21] Garcia, C. D., Liu, Y., Anderson, P., Henry, C. S., *Lab Chip* 2003, **3**, 331–335
- [22] Jackson, D. J., Naber, J. F., Roussel, T. J., Jr., Crain, M. M., Walsh, K. M., Keynton, R. S., Baldwin, R. P., *Anal. Chem.* 2003, **75**, 3311–3317.
- [23] Erickson, D., Sinton, D., Li, D., *Lab. Chip* 2004, **4**, 87–90.
- [24] Jiang, L., Jiang, X., Lu, Y., Dai, Z., Xie, M., Qin, J., Lin, B., *Electrophoresis* 2007, **28**, 1259–1264
- [25] Martin, R. S., Gawron, A. J., Lunte, S. M., Henry, C. S., *Anal. Chem.* 2000, **72**, 3196–3202.
- [26] Lee, Y.-J., Kim, H.-H., Hatori, H., *Carbon* 2004, **42**, 1053–1056.
- [27] Desmond, D., Lane, B., Alderman, J., Hill, M., Arrigan, D. W. M., Glennon, J. D., *Sens. Actuators, B* 1998, **48**, 409–414.
- [28] Castano-Alvarez, M., Fernandez-Abedul, M. T., Costa-Garcia, A., *J. Chromatogr. A* 2006, **1109**, 291–299.
- [29] Scherer, J. R., Liu, P., Mathies, R. A., *Rev. Sci. Instrum.* 2010, **81**, 113105-01–113105-07.
- [30] Diekmann, J., Adams, K. L., Klunder, G. L., Evans, L., Steele, P., Vogt, C., Herberg, J. L., *Anal. Chem.* 2011, **83**, 1328–1335.
- [31] Berg, C., Valdez, D. C., Bergeron, P., Mora, M. F., Garcia, C. D., Ayon, A., *Electrophoresis* 2008, 4914–4921.
- [32] Brito-Neto, J. G. A., da Silva, J. A. F., Blanes, L., do Lago, C. L., *Electroanalysis* 2005, **17**, 1207–1214.
- [33] Francisco, K. J. M., do Lago, C. L., *Electrophoresis* 2009, **30**, 3458–3464.
- [34] Elbashir, A. A., Aboul-Enein, H. Y., *Biomed. Chromatogr.* 2012. doi:10.1002/bmc.2729
- [35] do Lago, C. L., Juliano, V. F., Kascheres, C., *Anal. Chim Acta.* 1995, **310**, 281–288.
- [36] de Jesus, D. P., Brito-Neto, J. G. A., Richter, E. M., Angnes, L., Gutz, I. G. R., do Lago, C. L., *Anal. Chem.* 2005, **77**, 607–614.
- [37] Coelho, L. H. G., Gutz, I. G. R., *J. Brazil Chem. Soc.* 2011, **22**, 2157–2164.
- [38] Brito-Neto, J. G. A., da Silva, J. A. F., Blanes, L., do Lago, C. L., *Electroanalysis.* 2005, **17**, 1198–1206.
- [39] Coelho, L. H. G., Melchert, W. R., Rocha, F. R., Rocha, F. R. P., Gutz, I. G. R., *Talanta* 2010, **83**, 84–92.
- [40] Rocha, F. R., Coelho, L. H. G., Lopes, M. L. A., Carvalho, L. R. F., da Silva, J. A. F., do Lago, C. L., Gutz, I. G. R., *Talanta* 2008, **76**, 271–275.
- [41] Revermann, T., Gotz, S., Kunnemeyer, J., Karst, U., *Analyst* 2008, **133**, 167–174.
- [42] Saito, R. M., Brito-Neto, J. G. A., Lopes, F. S., Blanes, L., da Costa, E. T., Vidal, D. T. R., Hotta, G. M., do Lago, C. L., *Anal. Methods-Uk* 2010, **2**, 164–170.
- [43] Kasicka, V., Prusik, Z., Sazelova, P., Chiari, M., Miksik, I., Deyl, Z., *J. Chromatogr. B* 2000, **741**, 43–54.
- [44] Pumera, M., *J. Chromatogr. A* 2006, **1113**, 5–13
- [45] Xu, L., Hauser, P. C., Lee, H. K., *J. Chromatogr. A* 2008, **1214**, 17–22.
- [46] Xu, L., Hauser, P. C., Lee, H. K., *J. Chromatogr. A* 2009, **1216**, 5911–5916.
- [47] Kubáň, P., Seiman, A., Makarõtševa, N., Vaher, M., Kalju-rand, M., *J. Chromatogr. A* 2011, **1218**, 2618–2625.
- [48] Ding, Y. S., Garcia, C. D., Rogers, K. R., *Anal. Lett.* 2008, **41**, 335–350.
- [49] Rocha, F. R., da Silva, J. A. F., Lago, C. L., Fornaro, A., Gutz, I. G. R., *Atmos Environ.* 2003, **37**, 105–115.